energies

MDPI

Article

Performance Monitoring Algorithm for Detection of Encapsulation Failures and Cell Corrosion in PV Modules

Easter Joseph *, Pradeep Menon Vijaya Kumar, Balbir Singh Mahinder Singh and Dennis Ling Chuan Ching

Department of Fundamental and Applied Sciences, Universiti Teknologi PETRONAS, Seri Iskandar 32610, Perak Darul Ridzuan, Malaysia; pradeepmenonvkm@gmail.com (P.M.V.K.)
* Correspondence: easter.joseph@utp.edu.my

Abstract: This research work aims to develop a fault detection and performance monitoring system for a photovoltaic (PV) system that can detect and communicate errors to the user. The proposed system uses real-time data from various sensors to identify performance problems and faults in the PV system, particularly for encapsulation failure and module corrosion. The system incorporates a user interface that operates on a micro-computer utilizing Python software to show the detected errors from the PV miniature scale system. Fault detection is achieved by comparing the One-diode model with a controlled state retrieved through field testing. A database is generated by the system based on acceptable training data and it serves as a reference point for detecting faults. The user is notified of any deviations based on the threshold value from the training data as an indication of an error by the system. The system offers real-time monitoring, easy-to-understand error messages, and remote access capability, making it an efficient and effective tool for both users and maintenance personnel to manage and maintain the PV system.

Keywords: PV system; PV monitoring; fault detection algorithm; module corrosion; encapsulation failure

Citation: Joseph, E.; Vijaya Kumar, P.M.; Mahinder Singh, B.S.; Ching, D.L.C. Performance Monitoring Algorithm for Detection of Encapsulation Failures and Cell Corrosion in PV Modules. *Energies* **2023**, *16*, 3391. https://doi.org/10.3390/en16083391

Academic Editor: Sandro Nizetic

Received: 15 February 2023
Revised: 8 April 2023
Accepted: 10 April 2023
Published: 12 April 2023

1. Introduction

As many countries progress towards becoming developed nations, the exponential increase in global energy demand is inevitable. The predominant method of generating electricity at present is through fossil fuel combustion which includes petroleum, coal, and natural gases [1]. In line with the increase in consumer demand for these resources, the possibility of depletion and an increase in environmental pollution has dawned upon us. Thus, renewable energy is the best solution to provide and meet the growing energy demand. Among the available energy sources, solar energy provides a promising energy source as it can be considered an infinite energy source that can be harvested almost everywhere in the world [2]. Moreover, about 8.3×10^{17} kWh of energy received from the Sun can penetrate the atmosphere onto the Earth's surface which is approximately 10^4 times more than the current global energy demand.

Solar power is harnessed through photovoltaic (PV) cells, which are composed of P-N junctions. When sunlight falls on these junctions, electrons in the N-layer move to the P-layer of the junction diode, generating electricity. For effective use, solar power generation requires conditioning circuits and storage banks, which are incorporated into Solar Electricity Generating Systems (SEGSs). These systems consist of battery banks, charge controllers, and inverters, and are essential components for both standalone and grid-tie systems. Standalone systems are designed for small-scale applications such as domestic usage or emergency lighting in buildings during power outages, while grid-tie systems focus on power generation that is fed back into the grid.

The effectiveness of solar power generation depends not only on the efficiency of the PV panels but also on the efficiency of the entire power generation system. Many factors can affect the generation of power in SEGS, including module defects, electrical

losses, faults in the power lines and inverters, cloudy weather, dust accumulation, and local weather conditions [3]. These factors can significantly affect the ability of the PV system to generate power continuously, resulting in significant energy losses and substantial financial losses. The scope of this research is confined to small-scale off-grid connected phot PV systems, which emphasize the importance of monitoring systems with fault diagnostic abilities to promote long-lasting power generation and maximize their electrical output by detecting and communicating faults.

1.1. Photovoltaic Monitoring and Diagnostic Mechanism for Predictive Fault Detection

The significant expansion of PV generation facilities around the globe has led to a notable surge in the number of monitoring systems available. These systems are designed to efficiently deliver essential data to end-users, enabling them to plan for preventive maintenance and track the return on investment. Typically, the information conveyed by monitoring systems includes the output voltage and current of the PV, solar irradiance, relative humidity, and ambient temperature. As PV-based systems have become increasingly complex, it has become essential to add multiple sensors to measure the system's performance. The power generation of PV modules is critical, and failures in any subsystem can have adverse effects on the overall efficiency of the PV system [4]. All systems have a lifespan that is typically indicated by the manufacturer's specifications or experience gained from using the system or device. Despite the indicated lifespan, regular maintenance can improve the system's performance and extend its lifespan. Additionally, maintaining a maintenance record can help ensure the accuracy of measurements and system output. However, it can be challenging to determine the optimal time for maintenance when there is no previous record of the panel's output power under specific irradiation values.

To address this issue, a reference database of logged values must be utilized to enable the system to detect any deviation from previously achieved values. If a deviation is detected, the system alerts the user, who can then determine if maintenance activities are necessary or if the problem merely requires investigation at the affected panels. This approach is grounded in model-based techniques where the measured parameters are compared with theoretical data based on the One-diode equations. In this paper, the measured parameters are the controlled field data (training data) obtained by the PV miniature system. Many model-based techniques utilize power loss analysis, which employs solar irradiance and cell temperature to estimate the PV system's output power. Alternatively, empirical parameters such as fill factor, (FF), current short circuit (Isc), voltage open circuit (Voc), etc., which are calculated based on the shape of IV curves, can also be used [5].

The main focus of this research paper is to detect faults that commonly occur in PV systems, specifically encapsulation failures and module corrosion failures. Encapsulation failures happen when moisture and foreign materials enter the PV module's inner cavity due to the encapsulant material's degradation [6]. The most significant cause of this failure is discoloration and delamination (D and D), which is prevalent in areas with high temperatures and humidity. D and D leads to a poor conversion efficiency of solar energy to electricity by the PV modules [7]. Module corrosion, on the other hand, is caused by damage to the conductive surfaces of the PV module. The presence of a laminate edge can allow moisture to enter the module and lead to corrosion. When moisture is retained, it can increase the electrical conductivity of the materials used [7]. Corrosion can specifically target the metallic connections of PV cells, which can result in a leakage current and reduced performance. Additionally, corrosion can impact the adhesion between the metallic frame and the cells which leads to a reduction in series resistance [8].

1.2. Fault Detection Mechanisms

A few previously proposed fault detection mechanisms are presented. Several authors have been using model-based approaches that compare the analytically computed outputs with measured values and prompt a signal as an alarm [9]. Gagliarducci et al. proposes a cost-effective and flexible system for PV monitoring with the use of Global System for Mo-

bile (GSM) communication, which is also integrated with a PC that runs LabVIEW software. However, with the technology advancement, it has phased out the GSM technology [10]. Hazarika et al. proposed a solar PV system with an AT89S52 microcontroller to mitigate the efficiency drop due to factors such as dust or temperature increase. They added an automatic water-cooling system to address these issues, but it may require large volumes of water for high-voltage setups [11]. Chouder and Silvestre [12] utilized MATLAB/Simulink to create a model that detects and categorizes faults in a PV system by analyzing the DC power output, including thermal capture losses, miscellaneous losses, and current–voltage ratio. Silvestre's method involved comparing simulated and measured losses for detection, and error deviation between normal and faulty conditions for classification [13]. Stauffer et al. used measured and modeled DC power outputs to detect faults, but could not classify or locate them accurately, and false alarms can occur due to changes in irradiance [14]. Shimakage et al. used a comparison of past and present PV array conditions to detect partial shading and other faults [15].

In [16], the authors proposed a diagnostic theory to detect faults in PV systems based on three stages: data nodes with sensors, data acquisition, and data analysis. The parameters monitored during this process are voltage, current, and solar irradiation. To detect encapsulation failure, the actual maximum power point (MPP) value is compared with the value calculated by the reference PV module. If the actual MPP value is below the reference value, the PV panels should be cleaned and checked for damage. For module corrosion, the series resistance is compared between the actual and reference PV modules. The authors' proposal does not rely on any electronic controller or software. However, the algorithm used in the model must be able to evaluate the parameter of the electrical model to detect the failure mode. The authors of [17] proposed a simple and cost-effective method for diagnosing open-circuited and short-circuited PV modules in a string, which only requires temperature and irradiance sensors, as well as a power meter per string. The method uses a relative power value to compute an irradiance coefficient and compare the relative power of PV strings under different fault conditions. The study was conducted under controlled laboratory conditions and further field testing is needed to verify its effectiveness. Based on past research, the authors identified significant factors that affect relevant faults and plan to simulate them during field testing for an integrated performance monitoring system and fault detection in PV-based SEGS.

2. Methodology

This section discusses the components used for the assembly of the data-taking board, the diagnostic algorithm used in fault detection and preliminary fault classification, and experimental validation using an industrial device that was calibrated. The complete system can be categorized into two different units, namely the monitoring and data acquisition unit and the fault detection unit [18].

2.1. Monitoring and Data Acquisition Unit

The first stage was to determine the suitable meteorological and electrical parameters that needed to be monitored, followed by selecting the appropriate sensors capable of generating precise data for these identified parameters. Table 1 shows the detailed justification for the sensor selection [19]. Subsequently, an interfacing board was developed to effectively accommodate the necessary sensors and communicate with auxiliary devices via a serial communication protocol (SPI). This interfacing board serves as the monitoring and data acquisition unit that consisted of three separate modules, namely the main module, the sensor module, and the data storage module.

Table 1. Sensor selection criteria [19].

No.	Controlling Factor	Sensor	Description
1	Solar Radiation (W/m^2)	PV Cell 6 VDC rating	Using a reference cell to mimic a pyranometer by measuring the output DC voltage of the reference cell and a given pyranometer reading.
2	Output DC voltage (VDC)	Voltage divider circuit	The output voltage of the solar PV is much higher than that of what any controller can process. A voltage divider can parse the total voltage and make a portion of it smaller and thus readable.
3	Output DC Current (Amp)	ACS712 hall effect sensor	The sensor can measure up to 30 Amps and is a hall effect sensor thus making the electrical circuitry less invasive and modular.
4	Time (GMT+8)	DS1302 real-time clock module	This sensor is a clock chip that has an uninterrupted power supply in the form of a lithium cell thus being able to track time even when the power is switched off.
5	Light intensity (0~1023)	Light-dependent resistor (LDR)	This is the simplest and lowest costing light sensor that varies its resistance concerning the light intensity.
6	PV incline angle (°)	Potentiometer	Potentiometer or rheostat is a device with a rotating pot that at different positions provides different resistance values thus enabling the position to be controlled.
7	Temperature (°C) Humidity (%)	DHT11 temperature and humidity sensor	This circuit uses a temperature and humidity sensor multiplexed together to form the DHT11. The sensor returns 5 V data that requires a special library to process.

The main module is an ATMega 328 interfacing board that functions as the backup storage, display, and transfer unit. It retrieves data from the sensor module via the I2C communication protocol. The board is also equipped with a 16 × 2 LCD that can show sensor data, meteorological data, error messages, and the current time. Moreover, an SD card reader is included on the main module to provide a backup storage option for sensor information, error logs, and other customized user settings in situations where there is a Wi-Fi signal loss or disconnection. The sensor module contains all the required sensors to capture and interpret the meteorological and electrical data. An independent ATMega328 chip is utilized in this module solely to acquire and transmit the sensor data to the main module. The main module requests the specific sensor information required, and the sensor module maintains a queue to retrieve and execute the tasks in the designated sequence. The data storage module is designed to support the processing capability of both the main and sensor modules. Each ATMega chip has an integrated 1 KB EEPROM that is utilized for storing the program code. However, more complex processing tasks require larger code sizes, which can overload the chip and cause it to heat up quickly, increasing the likelihood of malfunction. To minimize the frequency of malfunctions, two extra EEPROMs were incorporated into the main module for storing codes in case additional sensor modules were added. Figures 1 and 2 show the complete monitoring system and its assembled miniature tracking system.

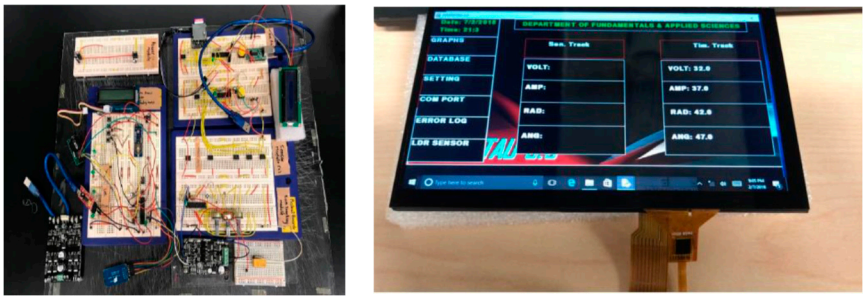

Figure 1. Final modular monitoring system.

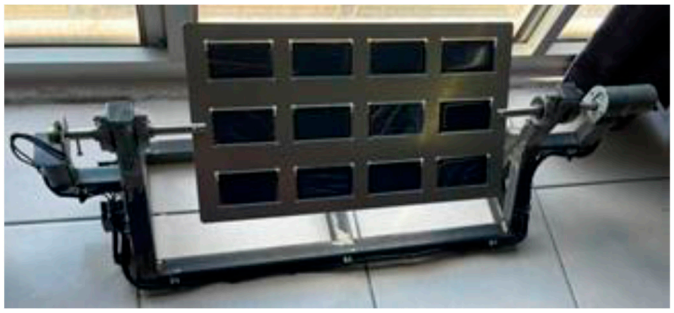

Figure 2. Final assembled miniature tracking system.

2.2. Fault Detection Unit

2.2.1. One-Diode Model

The one-diode model is always used to understand the electrical behavior of a PV cell and is also the preliminary step of fault detection [20]. The one-diode model is generally considered simpler and more computationally efficient compared with the two-diode model, which makes it more suitable for real-time monitoring and fault detection. In addition, the one-diode model is often sufficient for practical purposes and can provide a good approximation of the behavior of the PV system under various operating conditions. The relation between the environmental factors and the various parameters of the PV cell can be modeled mathematically using Equations (1)–(5), as shown in Figure 3. These equations show the module output current, I; photocurrent, I_{ph}; saturation current, I_0; reverse saturation current, I_{rs}; and current through the shunt resistor, I_{sh} [21].

$$I = N_p I_{ph} - N_p I_0 \left[exp^{\left(\frac{q(V+R_S)}{nKN_S T}\right)} - 1 \right] - I_{sh} \quad (1)$$

$$I_{ph} = [I_{sc} + k_i(T - 298)]\frac{G}{1000} \quad (2)$$

$$I_0 = I_{rs}\left(\frac{T}{T_n}\right)^3 exp\left[\frac{qE_g\left(\frac{1}{T_n} - \frac{1}{T}\right)}{nK}\right] \quad (3)$$

$$I_{rs} = \frac{I}{\left[e^{\left(\frac{qVoc}{nN_S KT}\right)-1}\right]} \quad (4)$$

$$I_{sh} = \left(\frac{V + IR_s}{R_{sh}}\right) \quad (5)$$

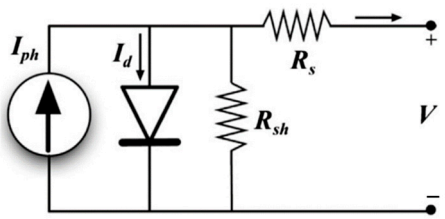

Figure 3. Cell equivalent model [22].

This research involved connecting three 5-V PV cells in a series to create a string, which was then connected in parallel to form a PV array as illustrated in Figure 2. When modeling a PV cell, it is typically assumed that the R_{SH} has a value approaching infinity and R_S is zero. However, a practical model must consider both series and shunt resistance to accurately represent the system. By simulating the PV cell using an equivalent circuit in MATLAB/Simulink, researchers aimed to obtain reference values that can be compared

with real-time measurement to achieve the most accurate results. The descriptions of each mathematical symbol are depicted in Table 2, while the datasheets of the reference PV module for this simulation are provided in Table 3.

Table 2. Details of mathematical symbols.

Symbol	Name	Value
k_i	Short-circuit current of a cell	0.0032
T	Operating temperature (K)	T
T_n	Nominal temperature (K)	298
G	Solar irradiance (W/m^2)	1000
q	Electron charge (C)	1.6×10^{-19}
n	The ideality factor of the diode	1.3
K	Boltzmann's constant (J/K)	1.38×10^{-23}
E_g	Band gap of semiconductor (eV)	1.1
R_s	Series resistance (Ω)	0.538
R_{sh}	Shunt resistance (Ω)	24.18

Table 3. Electrical characteristics data of reference PV module.

Symbol	Name	Value
I_{sc}	Short circuit current (A)	0.6 A
V_{oc}	Open circuit voltage (V)	5 Vdc
P_{max}	Rated power (W)	3.6 W
N_s	Number of cells in series	3
N_p	Number of PV modules in parallel	4

2.2.2. The Diagnostic Algorithm

The process of developing the algorithm begins by identifying the frequently occurring faults in PV that are often overlooked. A detailed analysis of these faults is carried out to understand their impact on PV's electrical parameters. The developed algorithm is incorporated into the data acquisition unit, which acts as a guideline for selecting appropriate sensors and programming codes to detect specific faults following a defined procedure. Fault detection and analysis were established using Human Machine Interface (HMI) through the Python™ programming platform. The embedded system with sensor networks collects data, which are sent to the Python™ program. Initially, training data are collected when the PV miniature system is in its initial state with optimal weather conditions. The training data aims to obtain values that closely match the simulated values obtained through MATLAB/Simulink. These simulated values serve to indicate how much the actual PV panel deviates from the ideal condition, allowing for manufacturing defects to be accounted for. If the user determines that the variance between the training data and simulated data is acceptable, the system then proceeds to record the training data to create a database, in which simulation values are no longer being used. The Python™ program then compares the real-time data with the previously collected training data to obtain the threshold value. The data are calculated using the mean difference in MPP between the training data and faults, as indicated in the Equation (6). The threshold value then can be set in the HMI. By following the sequence of the algorithm, the software constantly compares the threshold value with the MPP difference of the monitored data and signals an error if it detects any deviations. The MPP_{TD} and MPP_f are the MPP of training data and with fault.

$$MPP_{TH} = \frac{\sum(|MPP_{TD1} - MPP_{f1}| + |MPP_{TD2} - MPP_{f2}| + \cdots |MPP_{TDn} - MPP_{fn}|)}{n} \quad (6)$$

2.2.3. Encapsulation Failure and Module Corrosion

The experiment was configured by linking the interfacing board to the PV tracking system. The load used in this experiment was a 5-Vdc exhaust fan and data logging

time was limited between 9:00 a.m. and 3:30 p.m. where the Sun's light exposure and temperature are the highest and the best data would be able to be retrieved. The study aims to successfully detect two primary fault types: encapsulation failure and module corrosion. One way to detect errors caused by encapsulation failure is to compare the MPP obtained from training data with current data using solar irradiation as a reference point. Encapsulation failure can be detected by observing two conditions: (a) a single PV string covered with a translucent sheet, and (b) two PV strings covered with a translucent sheet, which are illustrated in Figure 4.

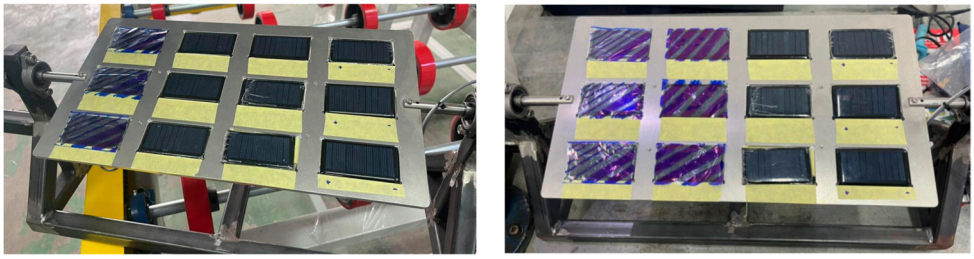

(**a**) (**b**)

Figure 4. (**a**) Case 1: single string; and (**b**) Case 2: two strings are covered with translucent sheets.

To understand module corrosion, the crucial factor affecting current output is an increase in series resistance, as noted in [23]. Therefore, the experimental setup involves using a 5 Vdc exhaust fan as the load to observe how changes in series resistance affect the amount of current received. Although the generated voltage remains constant, both power and current experience a drop, which is measurable by the monitoring system's ability to read both current and voltage. It should be noted that the crucial factor leading to a decrease in the MPP value when this fault occurs is the increase in series resistance across the entire PV array. Similarly, the IV and PV curves of the current data were compared with simulation curves to characterize this fault. Resistors were soldered in series to the PV cells in string to simulate the increase in the resistance of the string. Figure 5 displays two conditions that were observed: (a) modules using a 1-Ω resistor, and (b) PV modules using two 1-Ω resistors.

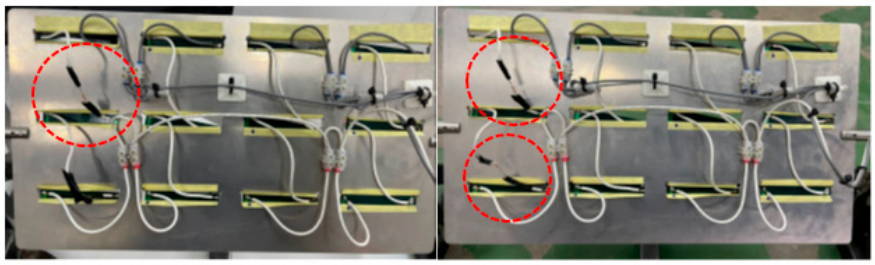

(**a**) (**b**)

Figure 5. (**a**) Case 3: one 1-Ω; and (**b**) Case 4: two 1-Ω resistors connected in series to the PV cells.

3. Results and Discussions

The controlled state from the PV miniature system is first obtained and reported. Figure 6 shows the reading of solar radiation of the PV reference cell and recorded maximum solar radiation of 850 W/m^2. The IV and PV curves of the controlled state were generated based on the amount of solar radiation and displayed in Figures 7 and 8. These data were then compared with the ideal model that had been simulated using MATLAB/Simulink software. Subsequently, the controlled state was compared with data retrieved from encapsulation failures and module corrosion faults. At the maximum solar radiation, the peak V and I obtained from the system were 12.11 Vdc with only 25 mA current, which differed from the ideal model. This discrepancy may be attributed to losses through wires

and manufacturing defects in the PV cell itself, which are not accounted for in the ideal one-diode model. Figure 7 enables the retrieval of the MPP value at a given radiation point, and any deviation from this value indicates the occurrence of an error.

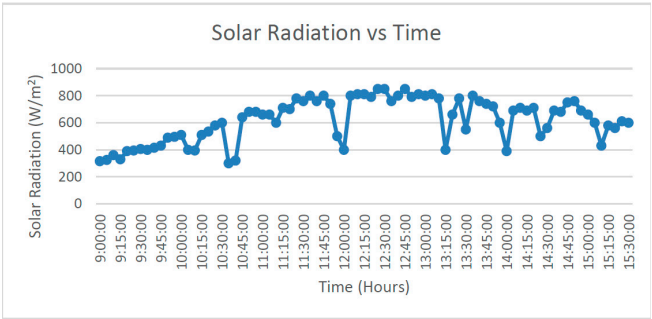

Figure 6. Solar radiation curve versus time of a PV reference cell.

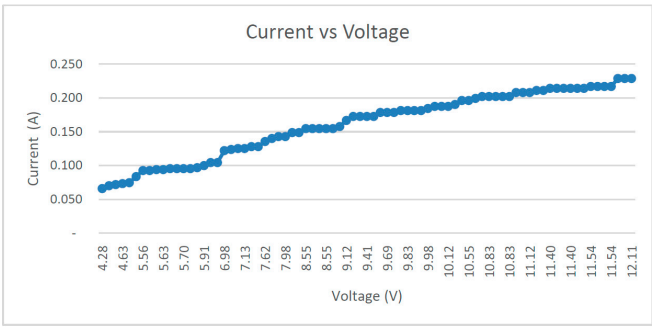

Figure 7. Graph of current vs. voltage of controlled state.

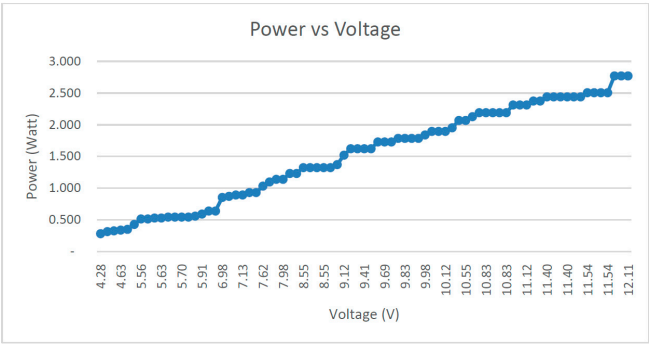

Figure 8. Graph of power vs. voltage of controlled state.

3.1. Characterization of Encapsulation Failure

The characterization of encapsulation failures centers around the MPP value of the PV curve, which is derived from data obtained during field testing. For Case 1 (single string covered with translucent sheets) and Case 2 (two strings covered with translucent sheets), solar radiation levels were initially determined on two different days by the PV reference cell attached to the PV miniature system. This results in two different solar radiation curves. Table 4 displays the values of solar radiation and the corresponding voltages generated by the controlled state and the two cases. These values were chosen because, during the experiments, the system generated two different voltages at a given radiation value. The reason for the variation is that the PV reference cell is located at the far end of the setup, and as clouds move non-linearly, fluctuations in values occur. To address this issue, the monitoring software automatically replaces the daily electrical parameter values with the highest recorded value. In this case, among the three conditions, Case 1

recorded the highest set of voltages, with readings of 8.84 Vdc and 8.71 Vdc at 660 W/m^2. In this scenario, even though a drop in the generated value may have signaled an error, the software ignores the new value of 8.71 Vdc while diagnosing for other potential faults. If no other faults are detected, the older value of 8.84 Vdc is used as the reference for comparison.

Table 4. Comparison of voltage generated at similar radiation values for three different states.

Experiment	Time	Solar Radiation (W/m^2)	Voltage (V)
Controlled state	10:25	580	8.06
	15:20	580	8.27
Case 1	11:10	660	8.84
	15:05	660	8.71
Case 2	11:20	612	7.43
	13:15	612	7.75

Table 5 provides proof that the current produced decreases as the amplitude of encapsulation failures increases. For encapsulation specifically, a decrease in voltage is always associated with a decrease in current. For fault detection, the software first verifies whether there is a decline in current, and if so, it then proceeds to monitor the voltage. If there is a significant drop in voltage, the software then compares the real-time MPP difference with the threshold MPP obtained from Equation (6). When the PV monitoring system detects a drop that goes beyond the threshold value, the HMI screen displays an error message, as shown in Figure 9, which indicates an encapsulation failure. It is important to note that the threshold is only used to determine the occurrence of fault if there is a significant voltage drop, in accordance with the sequence.

Table 5. Comparison of the current and power output of the PV miniature system for the three conditions at different solar radiations.

Solar Radiation (W/m^2)	Controlled State		Case 1		Case 2	
	Current (A)	Power (W)	Current (A)	Power (W)	Current (A)	Power (W)
510	0.211	1.056	0.192	0.959	0.182	0.910
600	0.300	1.520	0.281	1.404	0.269	1.345
700	0.414	2.069	0.387	1.934	0.373	1.864
790	0.527	2.635	0.497	2.483	0.481	2.403
810	0.554	2.770	0.523	2.614	0.506	2.532

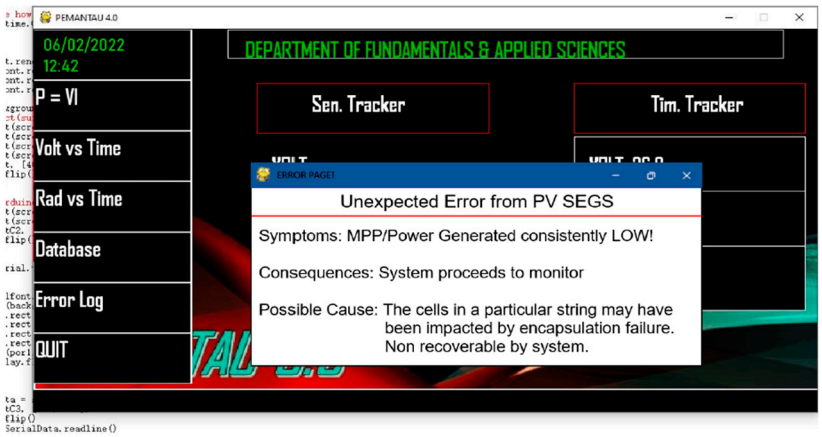

Figure 9. Error page showing detection of encapsulation failures.

3.2. Characterization of Module Corrosion

Module corrosion failure is closely related to the rise in the series resistance among cells in a string [24]. As the MPP is a critical factor in measuring circuit resistance, the main difference between this fault and encapsulation failures is a smaller decrease in the current value with the voltage value remaining the same. The overall load resistance of the entire PV array increases due to the rise in series resistance, which, according to Ohm's law, reduces the current value and thus the overall power. Consequently, the 5 Vdc exhaust fan rotates more slowly than it would under ideal conditions. Similarly, solar radiation was initially determined for the field testing that took place on two separate days. The highest solar radiation values recorded were 813 W/m^2 and 809 W/m^2.

Table 6 displays a comparison between the generated current at specific solar radiation levels. The data reveal that there is a consistent decline in current as the series resistance increases at all radiation levels. The selected data were chosen to eliminate the effects of clouds, which can cause non-uniform drops in current. The results show that the current reduction is much smaller in Case 3 and Case 4 than in Case 1 and Case 2 for encapsulation failure. To detect a fault, the software starts by checking for a drop in current value and subsequently examines the voltage if a reduction is detected. In the absence of any significant changes in voltage, the software proceeds to observe variations in resistance. If there is a surge in the resistance value, the system calculates the real-time MPP difference and compare it with the threshold, and if it surpasses the limit, the HMI exhibits an error message indicating that module corrosion has taken place. The accuracy of obtaining the threshold value is affected by a few reasons. One of these reasons is the size of the PV system, which uses miniature cells that are only capable of generating a small amount of power. As a result, a small mean difference in MPP is expected between the training data and the faulty data. While the small threshold value and unpredictable changes in irradiance may increase the likelihood of false alarms, the important factor in detecting and distinguishing faults is the drop in electrical parameter values, which is unique to each type of fault.

Table 6. Comparison of the current output of the PV miniature system for the three conditions at different solar radiations.

Solar Radiation (W/m^2)	Controlled State Current (A)	Case 3 Current (A)	Case 4 Current (A)
500	0.125	0.121	0.113
560	0.146	0.139	0.131
600	0.159	0.151	0.143
710	0.210	0.183	0.175
800	0.214	0.210	0.202

The fault detection algorithm of the python HMI uses a structured C-code with a top-down execution approach. Figure 10 illustrates the flow chart for this algorithm. The system collects data from the main module and checks for encapsulation failure continuously. If this fault is detected, an error window appears, and the program proceeds to check for module corrosion rather than rendering the PV array. If the system identifies a fault due to module corrosion, it displays an error window in front of the previous one, as shown in Figure 11. The detection of faults in the PV system alerts users to their occurrence and prompts the need for appropriate actions. Users are responsible for deciding whether to halt or proceed with power generation, as the system may operate with low performance despite the faults present. Consecutively, if an encapsulation failure is not detected, the program proceeds to check for module corrosion and follow similar steps to identify errors. The program runs continuously in the system for fault detection.

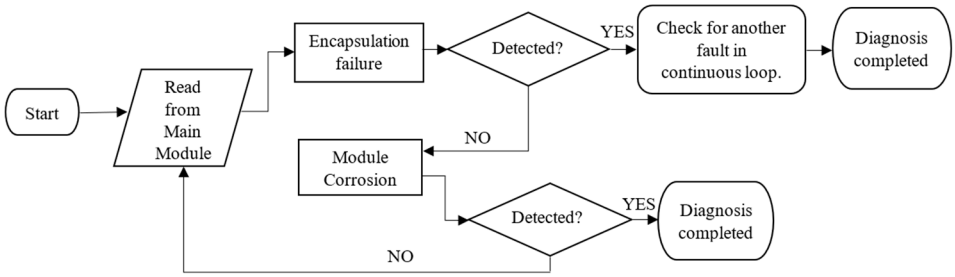

Figure 10. Flow chart for the python HMI fault detection algorithm.

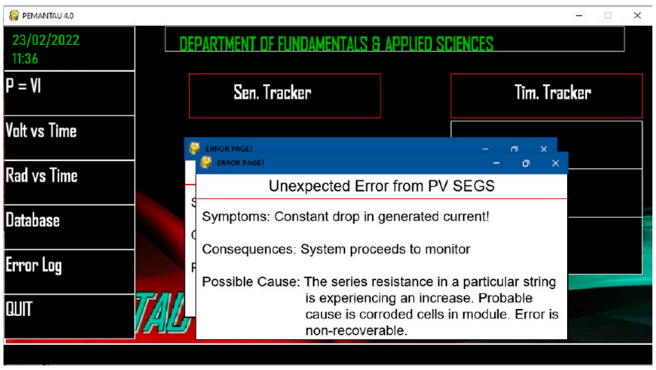

Figure 11. HMI screen message for module corrosion.

4. Conclusions

This study aimed to develop a monitoring system that can detect common faults that are often overlooked in PV modules. The researchers designed a custom-fabricated PV miniature system to test how module corrosion and encapsulation failure affect the PV's electrical parameters. Identifying faults and understanding their effect on the electrical parameters is paramount in developing the diagnostic algorithm. The algorithm uses training data to compare with simulation data obtained through MATLAB/Simulink. The training data were collected when the PV panel was in its initial state and optimal weather conditions. The comparison is expected to show deviations, and the HMI software communicates the magnitude of these deviations to the user to determine whether they are acceptable. The acceptable training data are used to create a database to compare against real-time data (faults). The threshold value is determined by calculating the mean difference in MPP between the training data and faults. Any deviations from the threshold value signal an error to the user. Based on the experimental results, the proposed monitoring system was effective in detecting faults through PV's electrical parameters such as voltage, current, and power of any PV module. However, there is room for improvement, such as adding more sensors to detect other types of faults and improving the analysis tools to provide more detailed information. Detecting faults early on can help ensure long-term energy efficiency gains and cost savings, ultimately leading to a more sustainable and reliable energy source.

Author Contributions: Conceptualization, P.M.V.K. and B.S.M.S.; methodology, P.M.V.K.; software, P.M.V.K.; validation, P.M.V.K., E.J., B.S.M.S. and D.L.C.C.; formal analysis, P.M.V.K. and E.J.; investigation, P.M.V.K.; resources, P.M.V.K.; data curation, P.M.V.K. and E.J.; writing—original draft preparation, P.M.V.K.; writing—review and editing, E.J. and D.L.C.C.; visualization, P.M.V.K.; supervision, B.S.M.S. and D.L.C.C.; project administration, E.J.; funding acquisition, E.J. All authors have read and agreed to the published version of the manuscript.

Funding: This research work is funded by the Yayasan Universiti Teknologi PETRONAS (YUTP) (015LC0-294).

Conflicts of Interest: The authors declare no conflict of interest.

References

1. Armaroli, N.; Balzani, V. The Future of Energy Supply: Challenges and Opportunities. *Angew. Chem. Int. Ed.* **2007**, *46*, 52–66. [CrossRef] [PubMed]
2. Mekhilef, S.; Safari, A.; Mustaffa, W.; Saidur, R.; Omar, R.; Younis, M.A. Solar energy in Malaysia: Current state and prospects. *Renew. Sustain. Energy Rev.* **2012**, *16*, 386–396. [CrossRef]
3. Mellit, A.; Tina, G.M.; Kalogirou, S.A. Fault detection and diagnosis methods for photovoltaic systems: A review. *Renew. Sustain. Energy Rev.* **2018**, *91*, 1–17. [CrossRef]
4. Catelani, M.; Ciani, L.; Cristaldi, L.; Faifer, M.; Lazzaroni, M. Electrical performances optimization of Photovoltaic Modules with FMECA approach. *Measurement* **2013**, *46*, 3898–3909. [CrossRef]
5. Davarifar, M.; Rabhi, A.; El-Hajjaji, A.; Dahmane, M. Real-time model base fault diagnosis of PV panels using statistical signal processing. In Proceedings of the 2013 International Conference on Renewable Energy Research and Applications (ICRERA), Madrid, Spain, 20–23 October 2013.
6. Lazzaroni, M.; Ferrari, S.; Piuri, V.; Salman, A.; Cristaldi, L.; Faifer, M. Models for solar radiation prediction based on different measurement sites. *Measurement* **2015**, *63*, 346–363. [CrossRef]
7. Park, N.; Jeong, J.; Kang, B.; Kim, D. The effect of encapsulant discoloration and delamination on the electrical characteristics of photovoltaic module. *Microelectron. Reliab.* **2013**, *53*, 1818–1822. [CrossRef]
8. Sharma, V.; Chandel, S. Performance and degradation analysis for long term reliability of solar photovoltaic systems: A review. *Renew. Sustain. Energy Rev.* **2013**, *27*, 753–767. [CrossRef]
9. Dhoke, A.; Sharma, R.; Saha, T.K. An approach for fault detection and location in solar PV systems. *Sol. Energy* **2019**, *194*, 197–208. [CrossRef]
10. Gagliarducci, M.; Lampasi, D.; Podestà, L. GSM-based monitoring and control of photovoltaic power generation. *Measurement* **2007**, *40*, 314–321. [CrossRef]
11. Hazarika, K.; Choudhury, P.K. Automatic monitoring of solar photovoltaic (SPV) module. *Mater. Today Proc.* **2017**, *4*, 12606–12609. [CrossRef]
12. Chouder, A.; Silvestre, S. Automatic supervision and fault detection of PV systems based on power losses analysis. *Energy Convers. Manag.* **2010**, *51*, 1929–1937. [CrossRef]
13. Silvestre, S.; Chouder, A.; Karatepe, E. Automatic fault detection in grid connected PV systems. *Sol. Energy* **2013**, *94*, 119–127. [CrossRef]
14. Stauffer, Y.; Ferrario, D.; Onillon, E.; Hutter, A. Power monitoring based photovoltaic installation fault detection. In Proceedings of the 2015 International Conference on Renewable Energy Research and Applications (ICRERA), Palermo, Italy, 22–25 November 2015.
15. Shimakage, T.; Nishioka, K.; Yamane, H.; Nagura, M.; Kudo, M. Development of fault detection system in PV system. In Proceedings of the 2011 IEEE 33rd International Telecommunications Energy Conference (INTELEC), Amsterdam, The Netherlands, 9–13 October 2011.
16. Cristaldi, L.; Faifer, M.; Lazzaroni, M.; Khalil, M.M.A.F.; Catelani, M.; Ciani, L. Diagnostic architecture: A procedure based on the analysis of the failure causes applied to photovoltaic plants. *Measurement* **2015**, *67*, 99–107. [CrossRef]
17. Gokmen, N.; Karatepe, E.; Celik, B.; Silvestre, S. Simple diagnostic approach for determining of faulted PV modules in string based PV arrays. *Sol. Energy* **2012**, *86*, 3364–3377. [CrossRef]
18. Triki-Lahiani, A.; Abdelghani, A.B.-B.; Slama-Belkhodja, I. Fault detection and monitoring systems for photovoltaic installations: A review. *Renew. Sustain. Energy Rev.* **2018**, *82*, 2680–2692. [CrossRef]
19. Rahman, M.; Selvaraj, J.; Rahim, N.; Hasanuzzaman, M. Global modern monitoring systems for PV based power generation: A review. *Renew. Sustain. Energy Rev.* **2018**, *82*, 4142–4158. [CrossRef]
20. Suman; Sharma, P.; Goyal, P. Analysing the effects of solar insolation and temperature on PV cell characteristics. *Mater. Today Proc.* **2021**, *45*, 5539–5543. [CrossRef]
21. Vengatesh, R.P.; Rajan, S.E. Investigation of cloudless solar radiation with PV module employing Matlab–Simulink. *Sol. Energy* **2011**, *85*, 1727–1734. [CrossRef]
22. Hong, Y.-Y.; Pula, R.A. Methods of photovoltaic fault detection and classification: A review. *Energy Rep.* **2022**, *8*, 5898–5929. [CrossRef]
23. Sangpongsanont, Y.; Chenvidhya, D.; Chuangchote, S.; Kirtikara, K. Corrosion growth of solar cells in modules after 15 years of operation. *Sol. Energy* **2020**, *205*, 409–431. [CrossRef]
24. Ndiaye, A.; Charki, A.; Kobi, A.; Kébé, C.M.; Ndiaye, P.A.; Sambou, V. Degradations of silicon photovoltaic modules: A literature review. *Sol. Energy* **2013**, *96*, 140–151. [CrossRef]